Fermilab

Fermi National Accelerator Laboratory
Technical Support Engineering
P.O. Box 500 - Batavia, Illinois - 60510

December 13, 1990

TO: SSC 50mm File

FROM: Jim Kerby, TS / Engineering

SUBJECT: Mechanical Analysis of the Vertically Split 50mm SSC Dipole

This paper presents results for finite element analyses of the vertically split yoke design for the 50mm SSC dipole, based on coil cross section W6733[1]. The results were first presented at the May 23, 1990 SSC Dipole Task Force meeting, at Brookhaven National Laboratory. The results for the horizontally spilt design, the BNL baseline dipole design, have been reported elsewhere[2]. Although related, and similar in appearance, the mechanics of the two designs are quite different. Rather than trying to ensure collar to yoke contact around the whole interface, the vertical split design only ensures contact at the horizontal region of the collar, leaving a clearance at the vertical 'poles' of the collar. The collars are deliberately oversized (horizontally) and undersized (vertically), so that shell tension is needed to close the yoke to yoke gap, and the yokes transmit the shell tension to the collars through the horizontal interference fit. The shell stress is a critical factor, as it determines the collar-yoke and yoke-yoke loads during assembly and operation of the magnet. Instead of constructing a structure with line to line fits when warm, the vertically split yoke magnet relies on localized interferences and clearances between the collar and yoke packs to achieve a more rigid support assembly after cooldown of the magnet. Furthermore, by creating a yoke-yoke compressive force greater than the expected Lorentz loading of the magnet, the yoke to yoke contact is always maintained, and the collar (and coil) motion due to excitation is reduced.

The goals of the mechanical analysis are then: 1) to minimize the coil motion under Lorentz loading, 2) maintain compressive loads between the collar and yoke at all times, 3) allow for a vertical collar to yoke clearance at all times, and 4) ensure the yoke to yoke split is closed after skinning of the cold mass. To achieve these goals, the finite element model has been used to determine the shape of the outside collar surface, the shell thickness and prestress necessary to close the yoke split when warm, the acceptable ranges of yoke taper (which allows for proper mating of the yoke halves due to bending of the iron during assembly), and the desired shape of the coil cavity in the collar lamination for proper conductor placement after cooldown. The effect of an internal pressure on the shell, simulating quench conditions, has also been investigated.

MODEL

The 2-D ANSYS model used for these calculations is shown in figure 1. As can be seen from the different mesh patterns, the model is actually a composite. The coil and collar mesh patterns are taken directly from the horizontally split yoke design[2], with a few modifications in the treatment of the coil system (a discussion of this change is documented elsewhere[3], but the differences are small). The yoke and shell meshes were then generated to allow for the proper treatment of the yoke-collar interface necessary with the vertical split. Although not particularly esthetically pleasing, neither of the two meshes cause any numerical distortions. A great thanks is due to Jon Turner and Giancarlo Spigo of the SSC Laboratory, for allowing use of their work in the generation of the coil and collar sections and the calculations of the Lorentz loads used in this model.

A number of assumptions are made in the model, including constant, isotropic, and elastic material properties, frictionless contact surfaces, plane stress analysis, and Lorentz loads calculated using infinite permeability iron. Collar to yoke interference is assumed only until an azimuthal angle of 30°, after which the surfaces are free with respect to one another.

RESULTS

Results are presented for four assembly and operational steps, namely Collaring, which simulates the collared coil after removal from the collaring press, Skinning, which simulates the completed cold mass after removal from the yoking press, Cooldown, which simulates the conditions of the magnet at 0 T, 4°K, and Excitation, which simulates the magnet at 6.9T, 4°K. Tabulated data show the radial deflections of the collar outer edge at the horizontal and vertical planes, while plots show the loading at the collar-yoke and yoke-yoke interfaces, and the shell tensile load.

1. Effect of Shell Stress

Calculations were made for cases of varying shell stress, to determine the minimum tensile load necessary, and the allowable range of stress in the shell while ensuring magnet operation. Table 1 shows the calculated deflections for each case, while Figures 2 though 4 show the collar-yoke, yoke-yoke, and shell forces associated with each case at each load step. Aside from the shell stress, all other parameters were held constant.

At the preload step, since the yoke and shell have not been applied yet, the deflections of the collared coil are identical for all cases. The vertical ovalization of the collar is expected, and the magnitude of these deflections agree well with those calculated in the horizontally split design, although differences do exist due to the differences in modeling techniques. Until the yoke split is closed, all of the shell load is transmitted by the yoke to the collar, which deflects radially inward horizontally and expands vertically. After yoke to yoke contact, collar motion stops, and further shell loads result in higher compressive yoke-yoke loads. This increasing collar-yoke load is apparent in Figure 2, while the yoke contact

appears to occur only for the highest shell stress case, resulting in a yoke-yoke load (Figure 3), decreased collar motion (Table 1) and a smaller increment of collar-yoke load increase (Figure 2). Further shell loading would result in higher yoke-yoke loads, but no increase in collar-yoke load or collar deflection.

Upon cooldown, the relative shrinking of the shell, yoke, collar and coil produce several effects. First, the shrinkage of the shell relative to the yoke causes the yoke interface to close for all cases of shell stress except the zero prestress case. Both the deflections, which show the collar to be in the nearly the same position for all shell loads, and the force plots, which show the identical collar-yoke load in each case support this. Differences in shell stress are reflected as differing yoke-yoke loads. The decrease in collar to yoke load from the preload case is due to the shrinkage of the collar away from the inside radius of the yoke, while the small differences in collar position are due to the differing shell stresses, which bend the yoke different amounts, and change the yoke-yoke interference at the vertical plane.

Finally, under excitation, the Lorentz loads are transmitted into increased collar-yoke loads, and offset by decreased yoke to yoke loads in all cases except where the shell initially had no prestress. When enough yoke to yoke compressive load exists after cooldown, the excitation of the magnet results in a trading of loads, minimal collar deflections, and constant shell loads. Radial collar deflections due to excitation are 0.018 mm (0.7 mils) horizontally and 0.032 mm (-1.25 mils) vertically, less than those predicted for the horizontally split design under the same conditions. The zero prestress shell case also shows an increase in collar-yoke load, although smaller since the increased horizontal deflection of the collar in this case results in more of the excitation load being resisted by the stiffness of the collar packs themselves, with less of the total Lorentz load being transmitted to the shell by the yoke. Using the criterion of yoke interface closure when warm, these results suggest a 4.9 mm (0.195 in) shell prestressed to about 151.7 MPa (22.0 ksi) will close the yoke gap and provide the desired collar-yoke loading.

2. Effect of Shell Thickness

In another comparison, the shell thickness was increased from 4.9 mm (0.195 in) to 6.35 mm (0.250 in) to investigate the effect on the support of the coil. The predicted shell tensile loads at room temperature were 117.9 MPa (17.1 ksi) and 110.3 MPa (16.0 ksi), respectively, while all other parameters were held constant. Displacement results are shown in Table 2, with forces in Figures 5 through 7. The 4.9 mm shell results are the same as those presented in Section 1. The predictions show the increased thickness provides enough additional support to close the yoke interface (the thinner shell results in an interface that is just open), and increased loading due to cooldown, as expected. However, the loading of the thinner shell with cooldown also results in yoke interface closure, so that with excitation there is no difference in mechanical performance. Although a thicker shell provides slightly increased stiffness and decreases the shell stress necessary to close the yoke split, it does not appear to provide a great mechanical advantage over a properly stressed thinner shell, in this design.

3. Effect of Coil Preload

The compressive preload applied to the coil has also been varied between 48.3 MPa (7.0 ksi) and 89.6 MPa (13.0 ksi) to examine the effect on the system mechanics (Table 3, Figures 8 through 10). This provides a tolerances on the vertical gap and horizontal interference necessary between the collar and the yoke. The higher preload case is identical to the case described in section 1 where the yoke gap is closed after skinning (highest shell stress). Table 3 shows reduced collar deflections for the lower preload case (linear with coil preload), but after skinning the collar has reached essentially the same horizontal position, although the vertical deflection is still different due to the variation in coil stress. Since the collar is more horizontally oval when less coil preload is applied, more of the shell forces are applied to the collar, and less into compression of the yoke to yoke split (figures 8 and 9). The yoke-yoke interface is still closed, with plenty of margin, and after cooldown and during operation, no difference in operation of the magnets is predicted.

The modeling results show a maximum collar deflection in the vertical direction of 0.19 mm (7.58 mils) after skinning, suggesting that leaving an 0.20 mm (8 mil) radial gap would (just) allow for free motion between the collar and yoke in this region. However, historically, finite element models have underpredicted the collar deflections measured on actual magnets, and since this parameter does not severely affect collar stiffness, a 0.41 mm (16 mil) radial gap between the collar and yoke at the vertical has been chosen to ensure clearance between the two at all times. In contrast, the horizontal interference between the collar and yoke must be large enough to maintain collar to yoke contact after cooldown. In a free standing state, the outside collar edge would contract almost 0.07 mm (2.7 mils) more to helium temperatures than the inside radius of the yoke. The interference fit of the collar and yoke at the horizontal must allow for this differential to maintain the desired loading scheme, and the design interference of 0.14 mm (5.5 mils) radially should be more than adequate for this purpose.

4. Yoke Taper

A yoke taper of 0.03 mm (1.25 mils) along the mating surface (greater gap at the outer radius) was found to provide the best yoke to yoke mating when the bending of the yoke was accounted for after skinning. However, tapers from no taper to 0.08 mm (3 mils) produced no significant effect on magnet operation, so the definition of this parameter is not critical. Due to the parting plane location on the vertical, the presence of a gap at the yoke split is not expected to have a detrimental effect on the magnetic performance of the magnet.

5. Shaping of the Coil Cavity

Since the collar (and coil) move more in the horizontal direction than the vertical, and the multipoles of the magnet are strong functions of conductor

placement, the coil cavity can be shaped to account for the motion and minimize the multipoles during operation. By examining the motion of the coil in the model from the initial state to the cooldown stage, an estimate of these placement corrections can be made. Another computation, using a coil preloaded to 69.0 MPa (10.0 ksi) (the median of the acceptable range), was completed for this purpose. Deflections change by less than ±1 mil if the preload is at one or the other extreme from this case. For the 10 ksi case, the coil cavity deflections (cartesian coordinates, in mm with mils in parentheses) are as follows:

Inner Coil, Inner Midplane	-0.21 (-8.07)	0.25 (10.00)
Inner Coil, Inner Pole	-0.02 (-0.81)	0.05 (1.96)
Inner Coil, Outer Pole	-0.03 (-1.35)	0.01 (0.43)
Outer Coil, Inner Pole	-0.09 (-3.49)	0.03 (1.19)
Outer Coil, Outer Pole	-0.12 (-4.87)	-0.02 (-0.95)
Outer Coil, Outer Midplane	-0.26 (-10.25)	0.25 (10.00)

The 0.25 mm (10 mil) vertical deflections at the midplane are artifacts of the application of coil preload in the model. By correcting the collar design for the remainder of the coil deflections, optimal positioning of the conductor during operation can be assured.

6. Comparison with other models

These results can be corroborated by comparison with other models. As previously mentioned, good agreement with the collar deflections calculated by the horizontally split mechanical analysis has been achieved. A SAPIV model of the yoke and shell interaction under Lorentz loads for this geometry has also been reported[4]. A comparison of the vertical split predictions, the SAPIV model, and the deflections for a collar only (no yoke or shell support at any time) is shown in Table 4. The SAPIV model predicts a horizontal deflection of the yoke by 0.06 mm (2.5 mils) during excitation, while the vertical split model predicts a deflection of only 0.02 mm (0.7 mils). However, the SAPIV model does not account for the stiffness of the collar, which also resists the Lorentz load of the coil. The collar only case presented in Table 4 shows the collar to be a relatively stiff support member, having a non-negligible effect on the support structure. Summing the loads transmitted between the collar and the yoke show that only 45% of the total Lorentz load is transmitted to the yoke by the collar. A linear scaling of the SAPIV results by this amount reduces the predicted deflection to 0.03 mm (1.125 mils). Furthermore, the load is actually transmitted as a distributed load, instead of as a point load as used in the SAPIV model. Taking these two effects into account, good agreement is found between the two models.

7. Effect of Quench Pressures on Support System

Quenches produce high internal pressures on the cold mass shell, which could reduce the shell load on the yoke, also reducing the yoke to yoke loading and the collar to yoke loading. However, the design pressure for the SSC magnet, 2.1 MPa (300 psi), is low enough that the yoke to yoke loading changes by only

350.3 N/mm (2000 lb/axial inch). Quenches should have no effect on the cold mass mechanics.

CONCLUSIONS

The finite element model of the 50mm vertically split dipole gives good agreement on collar deflections with two other, independently created models. The results suggest that a 4.9 mm (0.195 in) shell, prestressed when warm to 151.7 MPa (22.0 ksi), will close the yoke to yoke gap. Oversizing the collar 0.14 mm (5.5 mils) horizontally, and undersizing the collar 0.41 mm (16 mils) vertically, will supply the necessary geometry to take full advantage of the vertically split yoke support mechanism. Furthermore, the coil cavity of the collar can be shaped to provide for optimum field quality during operation of the magnet.

REFERENCES

1. J. Morgan and R. Gupta, BNL.
2. J. Turner, "Mechanical Analysis of the W6733H Cross Section", MD-TA-143 (SSCL), May 1990.
3. J. Kerby, SSC-XX-XXX, (FNAL)
4. C. Goodzeit, "Structural Response of DSX201 Yoke and Shell (and Vertically Split Version) to Thermal and Lorentz Loads", April 23, 1990.

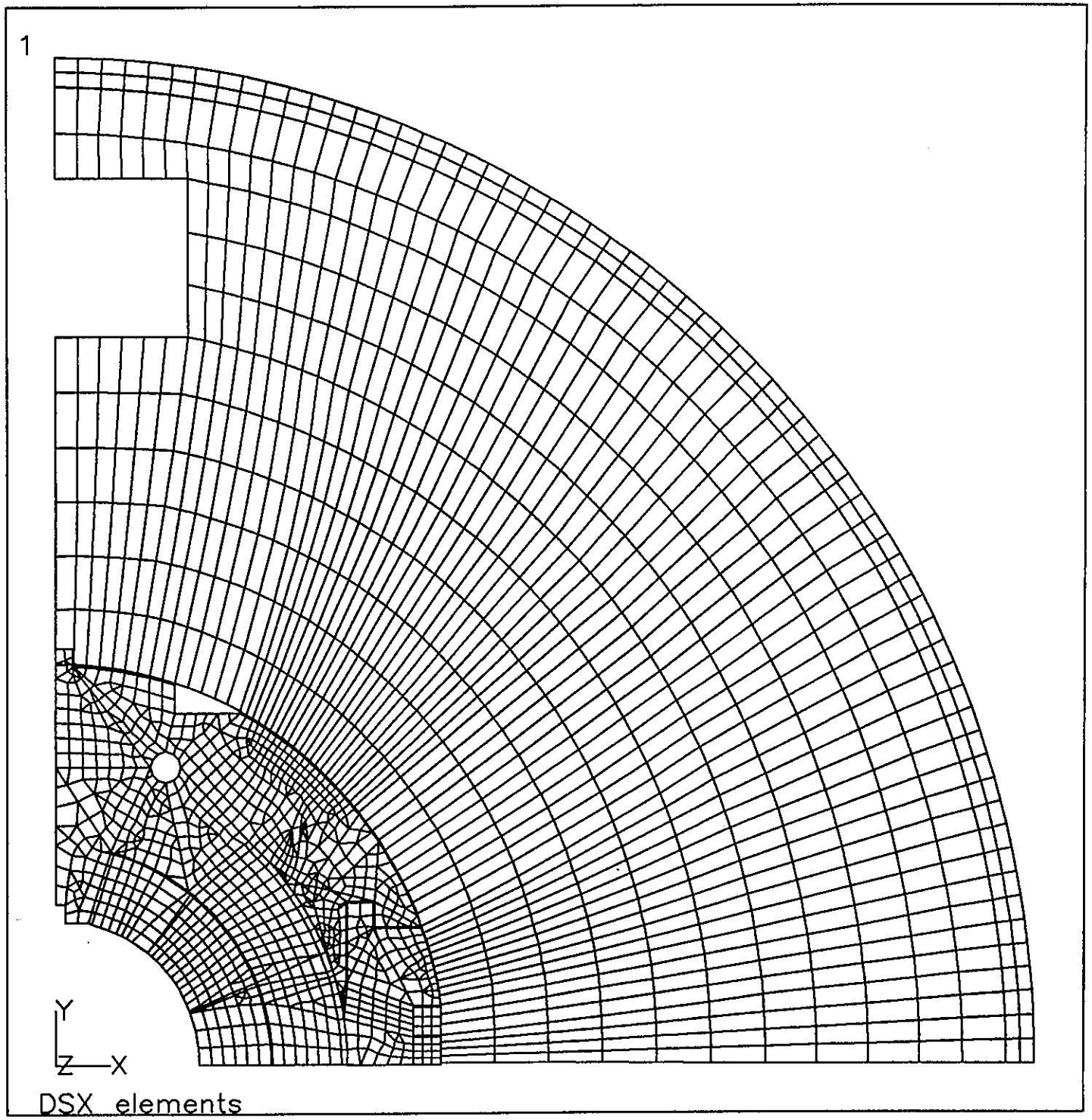

ANSYS 4.4
MAY 21 1990
07:20:33
PLOT NO. 1
PREP7 ELEMENTS
TYPE NUM

ZV =1
DIST=93.5
XF =85
YF =85

Figure 1

Table 1. Collar Radial Displacements

0.195" (4.90mm) Skin, 13ksi Coil Preload

mils (mm)

Preload	Horizontal	Vertical
Free Skin	-0.69 (-.017)	4.60 (.117)
8.1ksi Skin	-0.69 (-.017)	4.60 (.117)
12.5ksi Skin	-0.69 (-.017)	4.60 (.117)
17.1ksi Skin	-0.69 (-.017)	4.60 (.117)
24.8ksi Skin	-0.68 (-.017)	4.60 (.117)

Skinning	Horizontal	Vertical	ΔH	ΔV
Free Skin	-0.69 (-.017)	4.60 (.117)	0.00	0.00
8.1ksi Skin	-3.10 (-.079)	5.93 (.151)	-2.41	1.33
12.5ksi Skin	-4.39 (-.111)	6.65 (.169)	-3.70	2.05
17.1ksi Skin	-5.63 (-.143)	7.37 (.187)	-4.94	2.77
24.8ksi Skin	-5.98 (-.152)	7.58 (.193)	-5.30	2.98

Cooldown	Horizontal	Vertical	ΔH	ΔV
Free Skin	-11.68 (-.297)	-2.98 (-.076)	-11.0	-7.58
8.1ksi Skin	-11.77 (-.299)	-2.93 (-.074)	-8.67	-8.86
12.5ksi Skin	-11.81 (-.300)	-2.90 (-.074)	-7.42	-9.55
17.1ksi Skin	-11.86 (-.301)	-2.88 (-.073)	-6.23	-10.25
24.8ksi Skin	-11.91 (-.302)	-2.87 (-.073)	-5.93	-10.45

Excitation	Horizontal	Vertical	ΔH	ΔV
Free Skin	-9.21 (-.234)	-5.18 (-.131)	2.47	-2.20
8.1ksi Skin	-11.06 (-.281)	-4.15 (-.105)	0.71	-1.22
12.5ksi Skin	-11.11 (-.282)	-4.11 (-.105)	0.70	-1.21
17.1ksi Skin	-11.16 (-.284)	-4.09 (-.104)	0.70	-1.21
24.8ksi Skin	-11.21 (-.285)	-4.06 (-.103)	0.70	-1.19

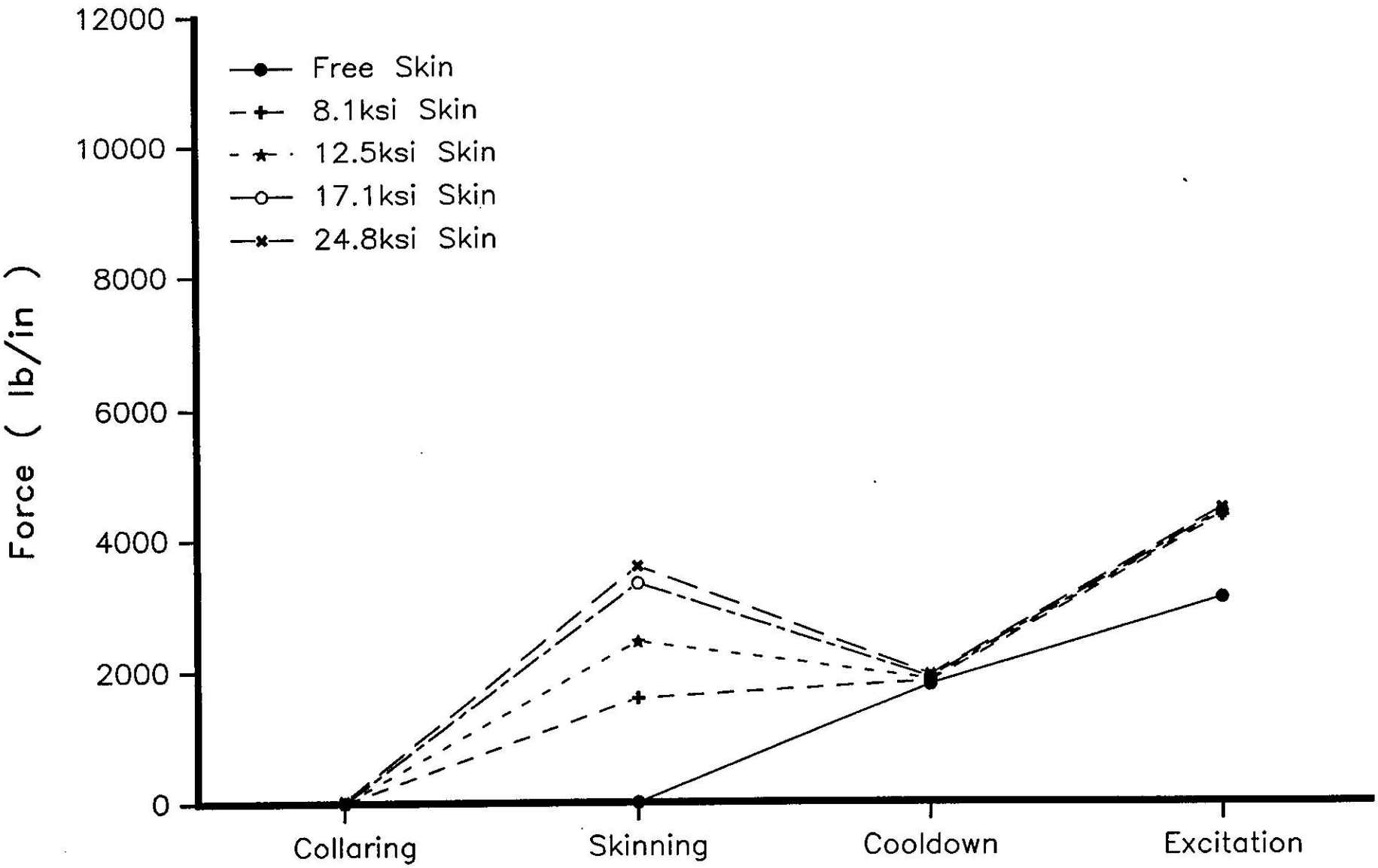
Collar / Yoke Forces
4.95mm (0.195") skin, varying warm skin stress
Force (lb/in)
12000
10000
8000
6000
4000
2000
0
Free Skin
8.1ksi Skin
12.5ksi Skin
17.1ksi Skin
24.8ksi Skin
Collaring
Skinning
Cooldown
Excitation

Figure 2

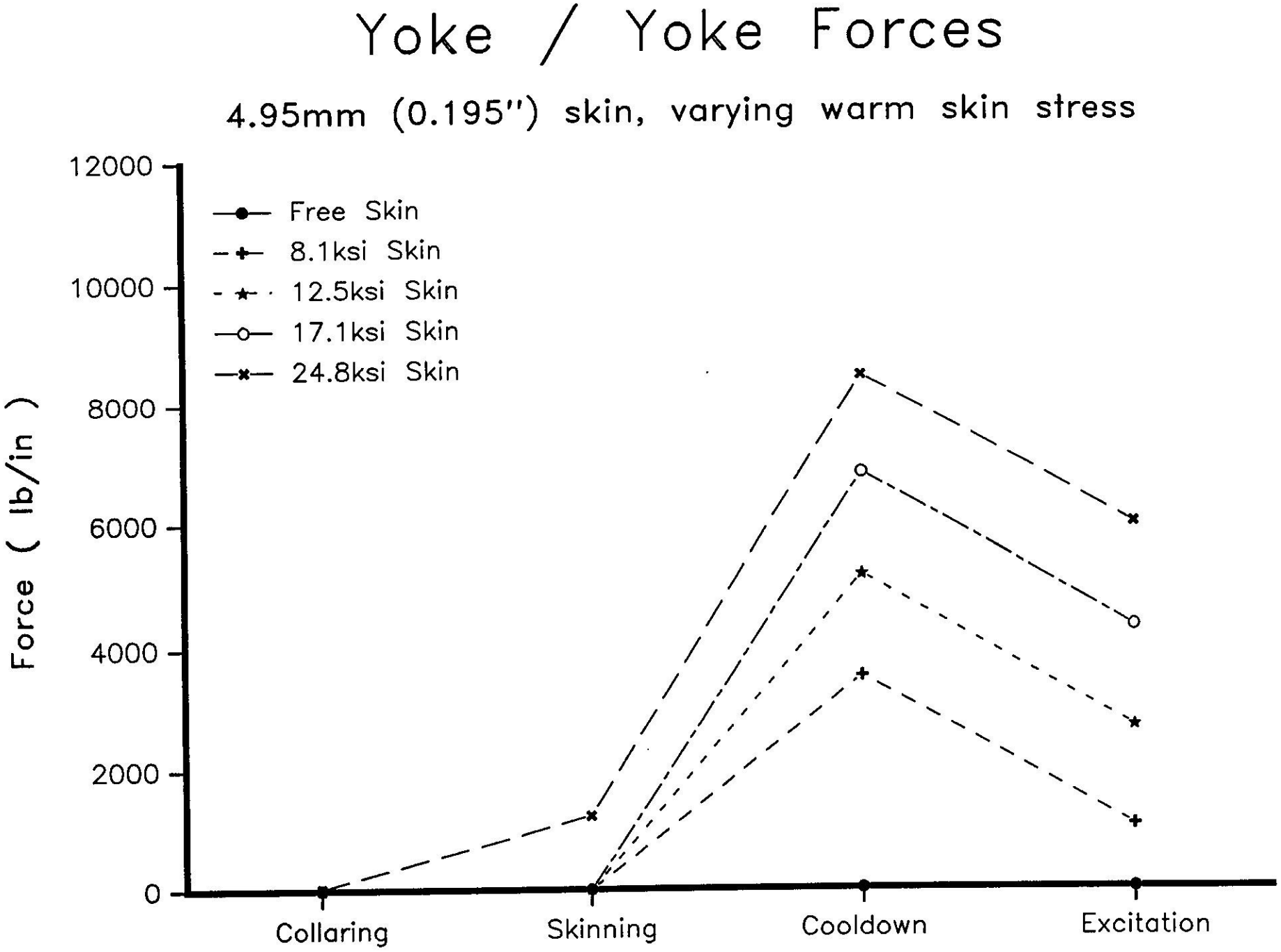
Yoke / Yoke Forces
4.95mm (0.195") skin, varying warm skin stress
Free Skin
8.1ksi Skin
12.5ksi Skin
17.1ksi Skin
24.8ksi Skin
Force (lb/in)
12000
10000
8000
6000
4000
2000
0
Collaring
Skinning
Cooldown
Excitation

Figure 3

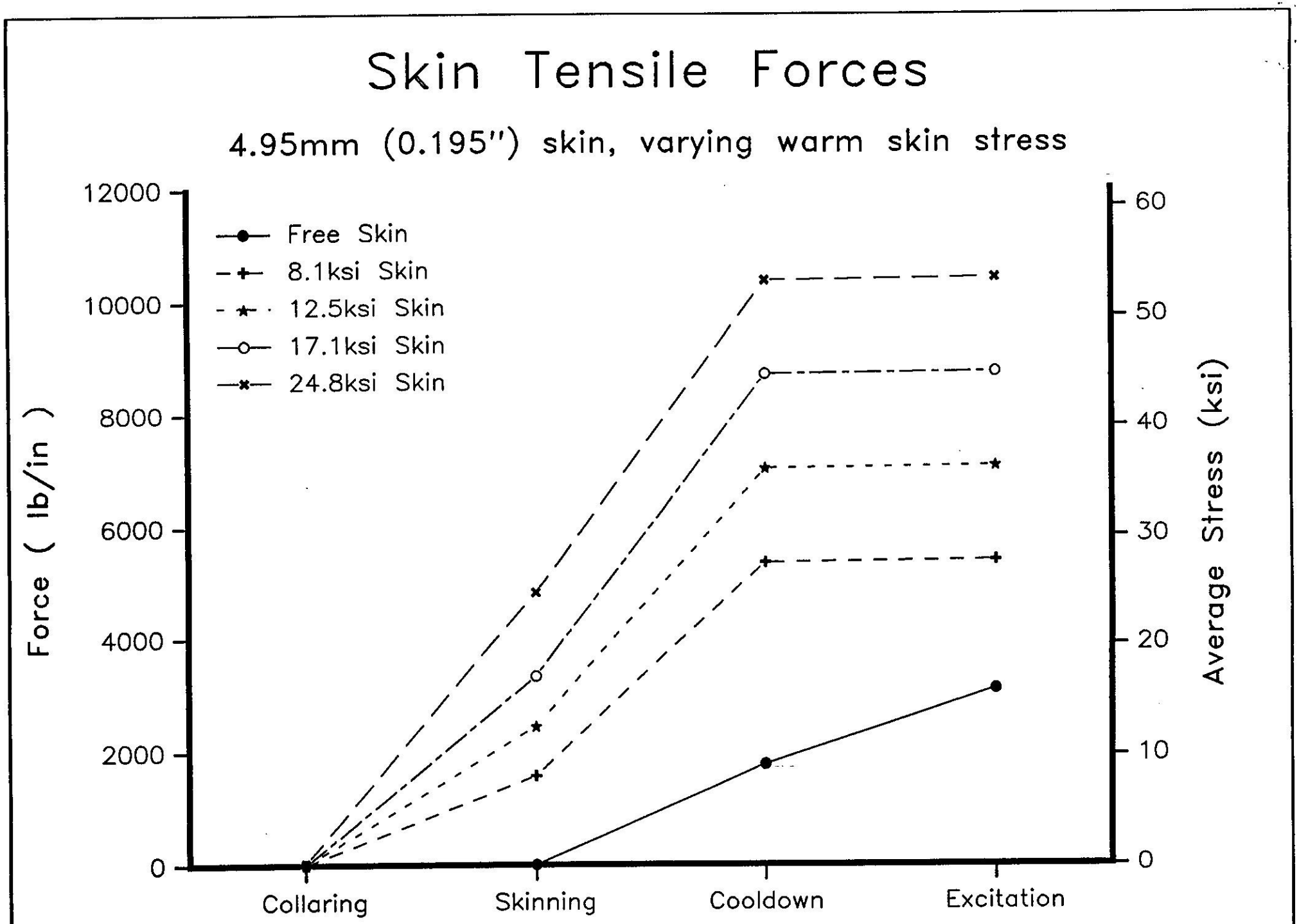
Skin Tensile Forces
4.95mm (0.195") skin, varying warm skin stress
Free Skin
8.1ksi Skin
12.5ksi Skin
17.1ksi Skin
24.8ksi Skin
Force (lb/in)
Average Stress (ksi)
12000
10000
8000
6000
4000
2000
0
60
50
40
30
20
10
0
Collaring
Skinning
Cooldown
Excitation

Figure 4

Table 2. Collar Radial Displacements

Increased Skin Thickness

mils (mm)

Preload	Horizontal	Vertical
0.195"/17.1ksi	-0.69 (-.017)	4.60 (.117)
0.250"/16.0ksi	-0.69 (-.017)	4.60 (.117)

Skinning	Horizontal	Vertical	ΔH	ΔV
0.195"/17.1ksi	-5.63 (-.143)	7.37 (.187)	-4.94	2.77
0.250"/16.0ksi	-5.95 (-.151)	7.56 (.192)	-5.27	2.96

Cooldown	Horizontal	Vertical	ΔH	ΔV
0.195"/17.1ksi	-11.86 (-.301)	-2.88 (-.073)	-6.23	-10.25
0.250"/16.0ksi	-11.93 (-.303)	-2.84 (-.072)	-5.98	-10.40

Excitation	Horizontal	Vertical	ΔH	ΔV
0.195"/17.1ksi	-11.16 (-.284)	-4.09 (-.104)	0.70	-1.21
0.250"/16.0ksi	-11.23 (-.285)	-4.05 (-.103)	0.70	-1.21

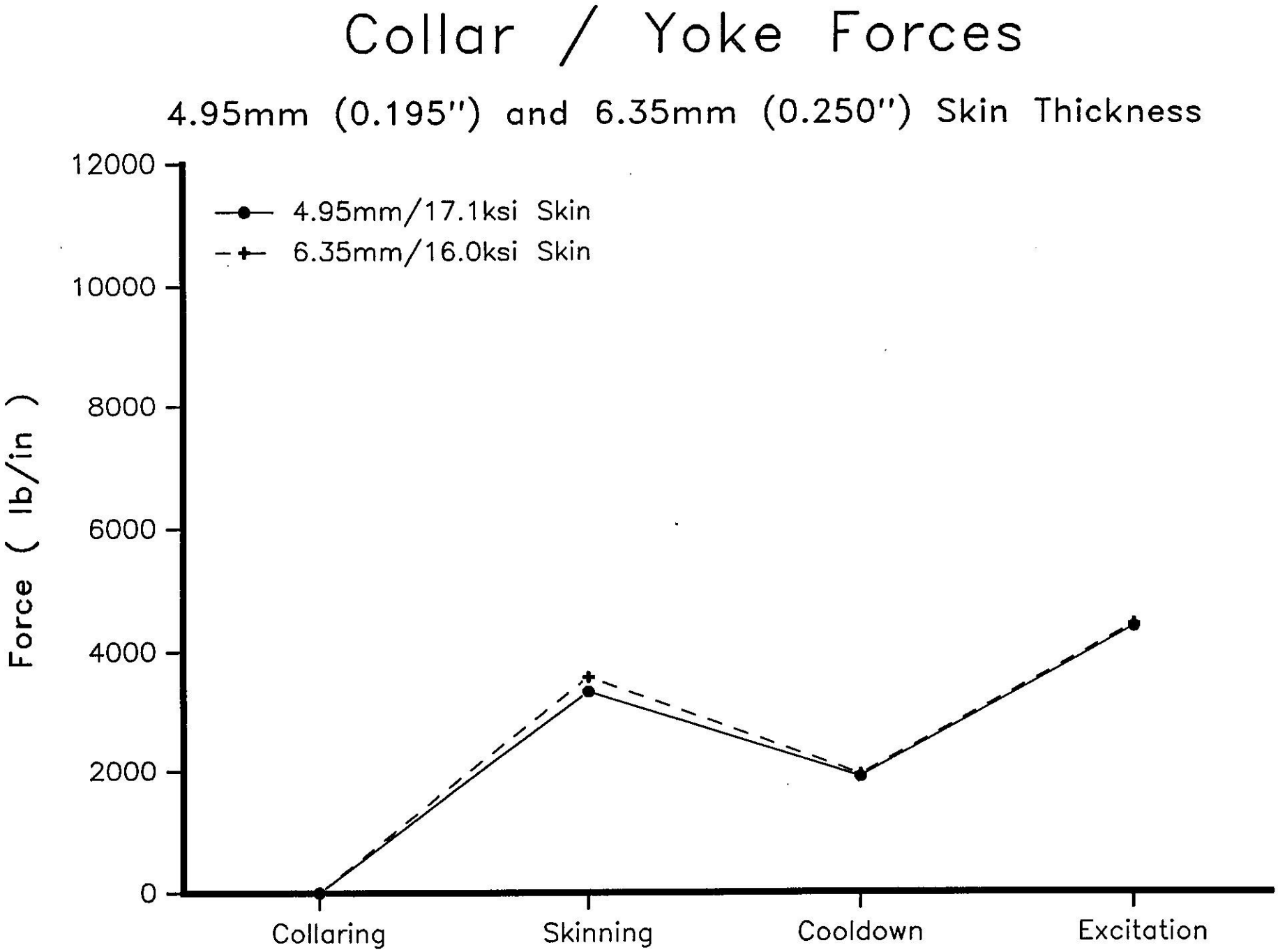
Collar / Yoke Forces
4.95mm (0.195") and 6.35mm (0.250") Skin Thickness
4.95mm/17.1ksi Skin
6.35mm/16.0ksi Skin
Force (lb/in)
12000
10000
8000
6000
4000
2000
0
Collaring
Skinning
Cooldown
Excitation

Figure 5

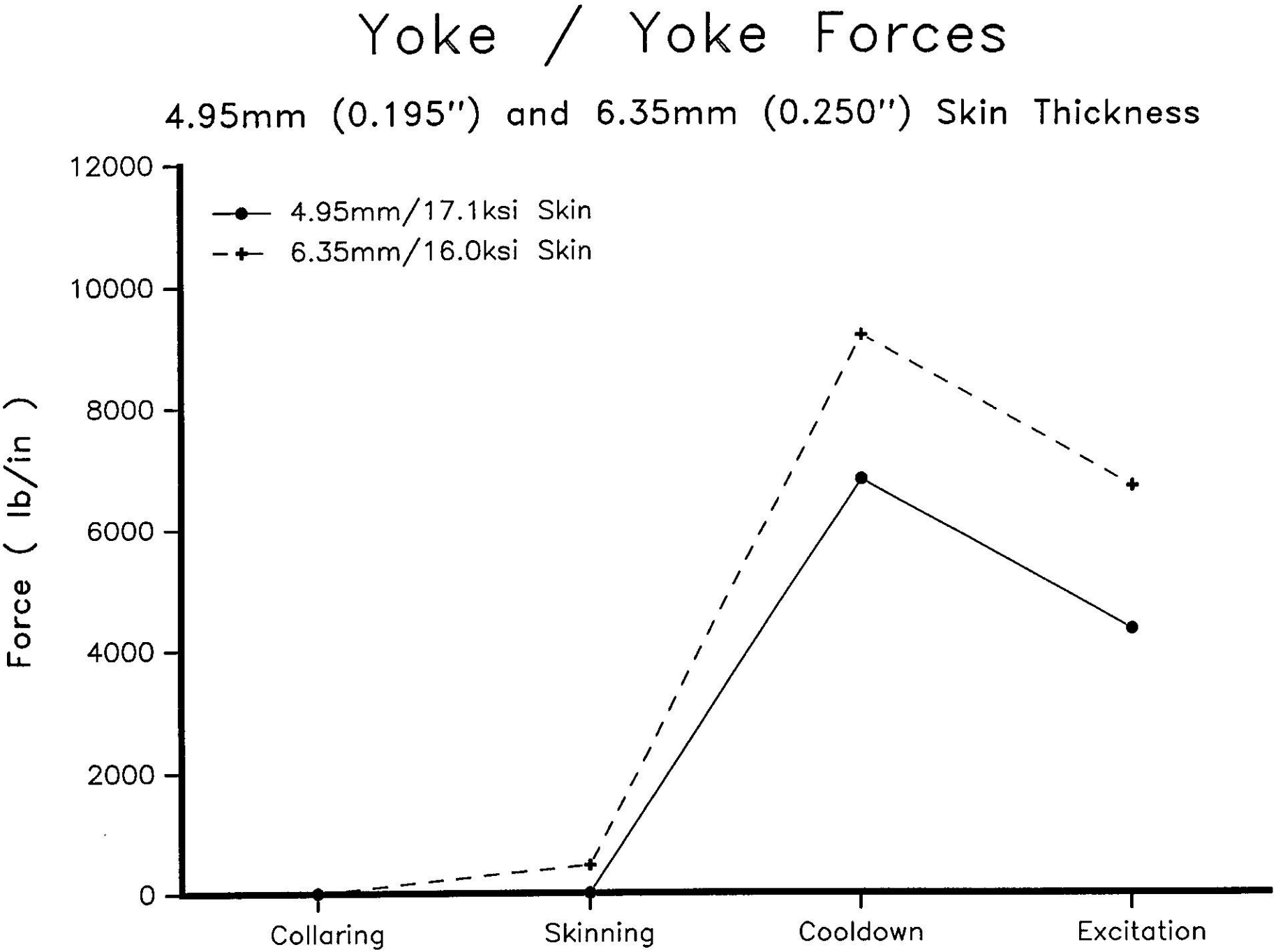
Yoke / Yoke Forces
4.95mm (0.195") and 6.35mm (0.250") Skin Thickness
4.95mm/17.1ksi Skin
6.35mm/16.0ksi Skin
Force (lb/in)
12000
10000
8000
6000
4000
2000
0
Collaring
Skinning
Cooldown
Excitation

Figure 6

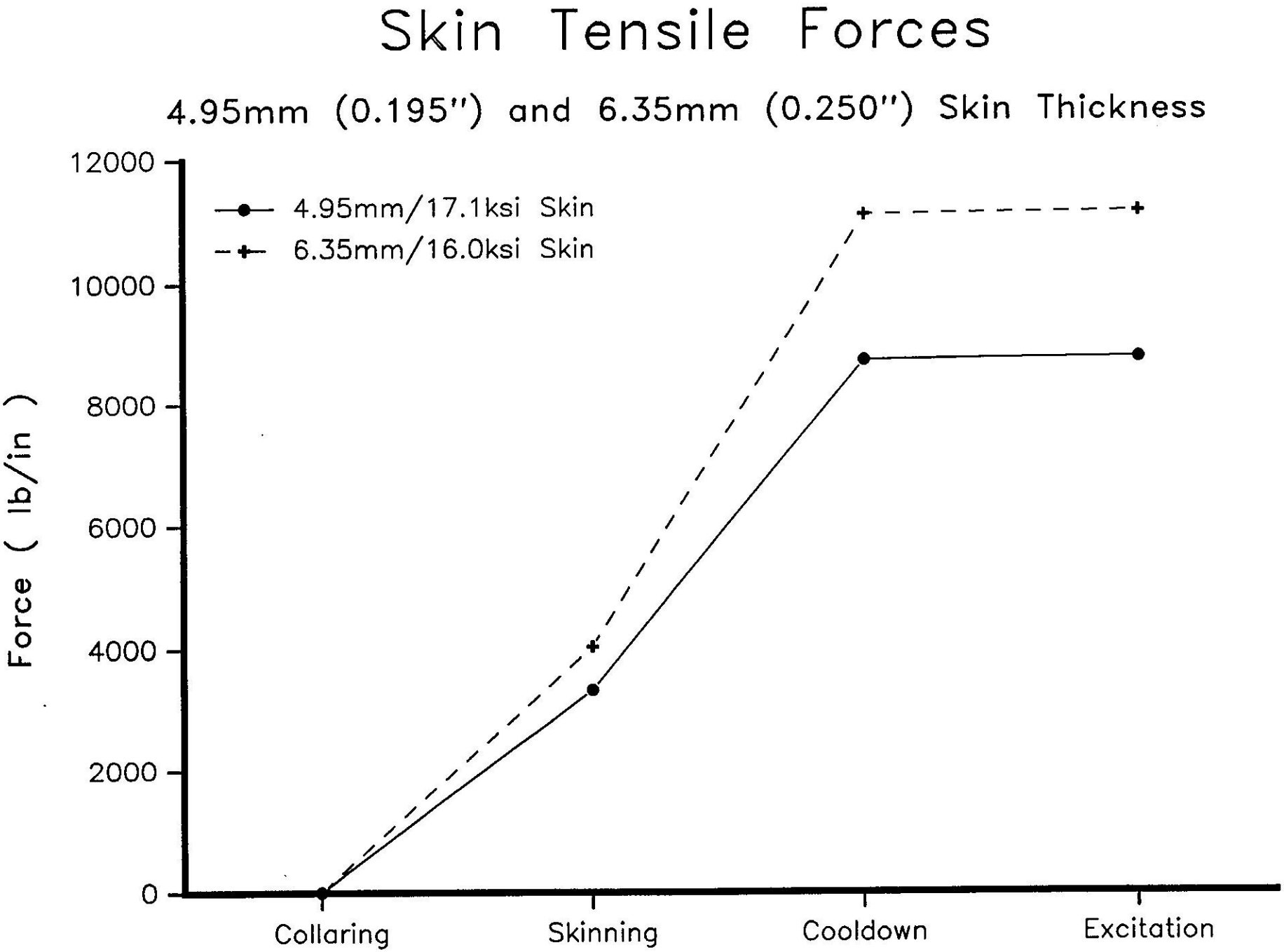
Skin Tensile Forces
4.95mm (0.195") and 6.35mm (0.250") Skin Thickness
4.95mm/17.1ksi Skin
6.35mm/16.0ksi Skin
Force (lb/in)
12000
10000
8000
6000
4000
2000
0
Collaring
Skinning
Cooldown
Excitation

Figure 7

Table 3. Collar Radial Displacements

0.195" (4.9mm) Skin 25 ksi Warm Prestress

mils (mm)

Preload	Horizontal	Vertical		
7. ksi coil	-0.37 (-.009)	2.48 (.063)		
13. ksi coil	-0.68 (-.017)	4.60 (.117)		
Skinning	Horizontal	Vertical	ΔH	ΔV
7. ksi coil	-5.83 (-.148)	5.71 (.145)	-5.46	3.23
13. ksi coil	-5.98 (-.152)	7.58 (.193)	-5.30	2.98
Cooldown	Horizontal	Vertical	ΔH	ΔV
7. ksi coil	-11.76 (-.299)	-4.77 (-.121)	-5.93	-10.48
13. ksi coil	-11.91 (-.302)	-2.87 (-.073)	-5.93	-10.45
Excitation	Horizontal	Vertical	ΔH	ΔV
7. ksi coil	-11.11 (-.282)	-5.94 (-.151)	0.65	-1.17
13. ksi coil	-11.21 (-.285)	-4.06 (-.103)	0.70	-1.19

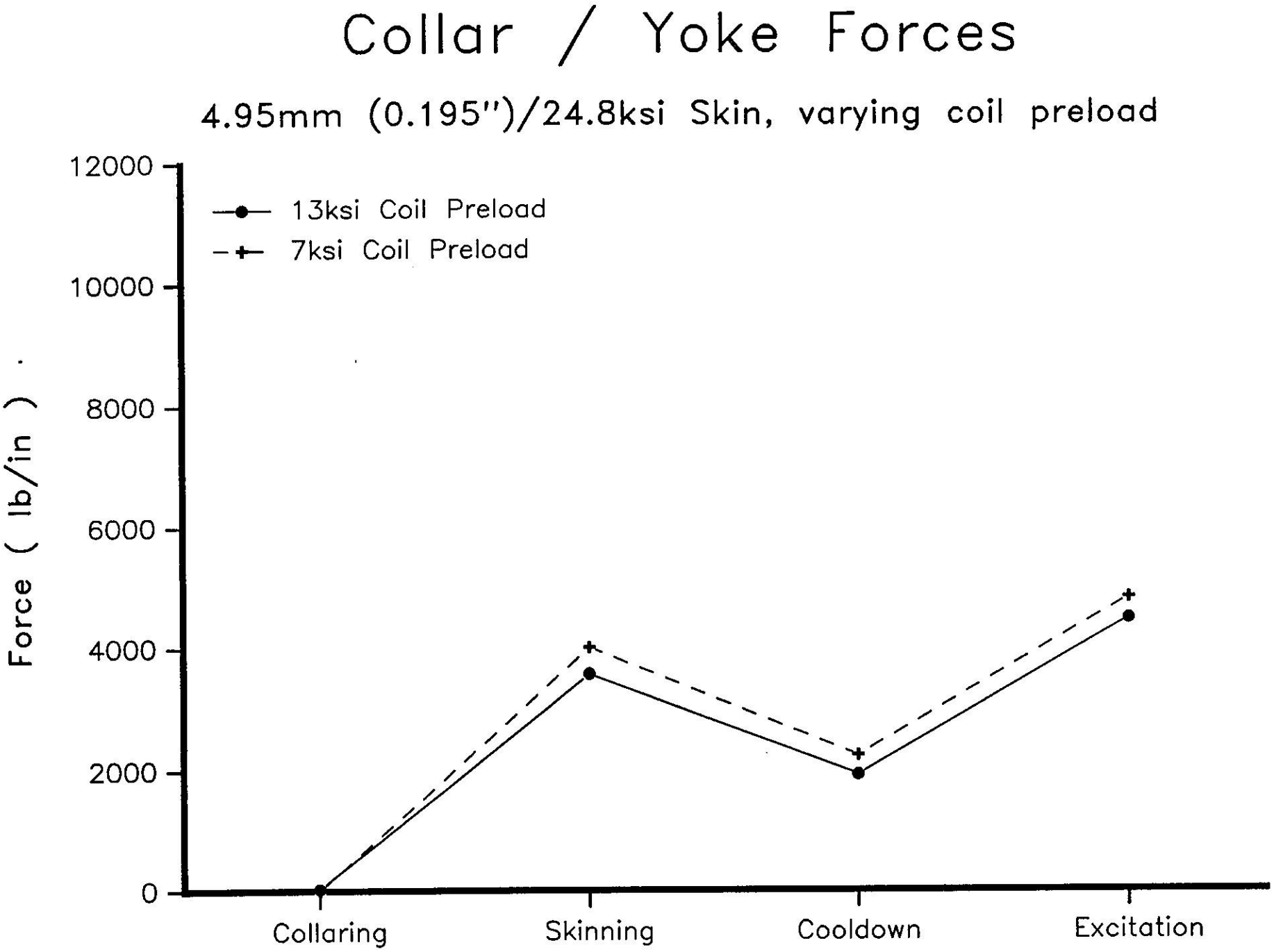
Collar / Yoke Forces
4.95mm (0.195")/24.8ksi Skin, varying coil preload
13ksi Coil Preload
7ksi Coil Preload
Force (lb/in)
12000
10000
8000
6000
4000
2000
0
Collaring
Skinning
Cooldown
Excitation

Figure 8

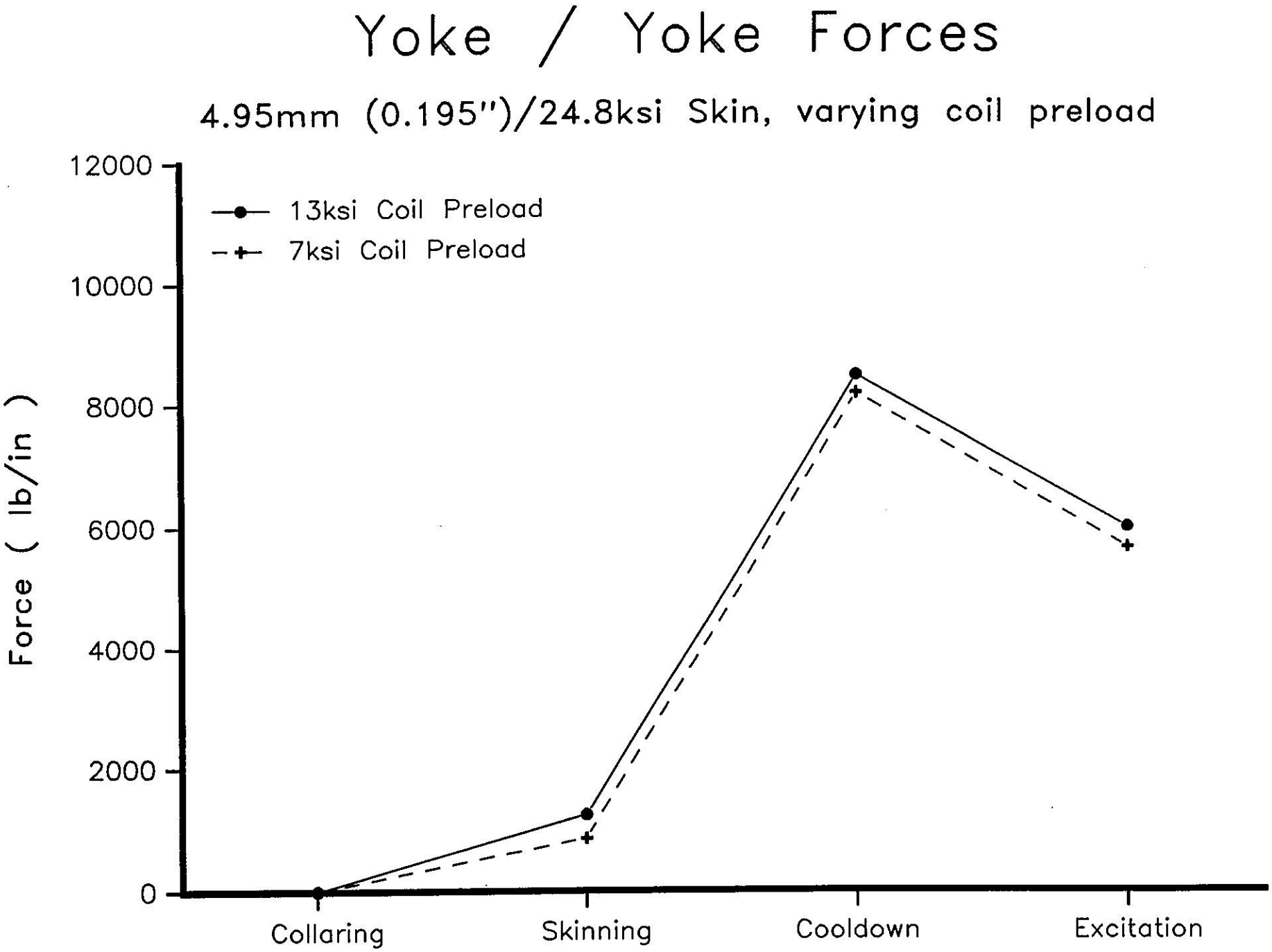
Yoke / Yoke Forces
4.95mm (0.195")/24.8ksi Skin, varying coil preload
13ksi Coil Preload
7ksi Coil Preload
Force (lb/in)
12000
10000
8000
6000
4000
2000
0
Collaring
Skinning
Cooldown
Excitation

Figure 9

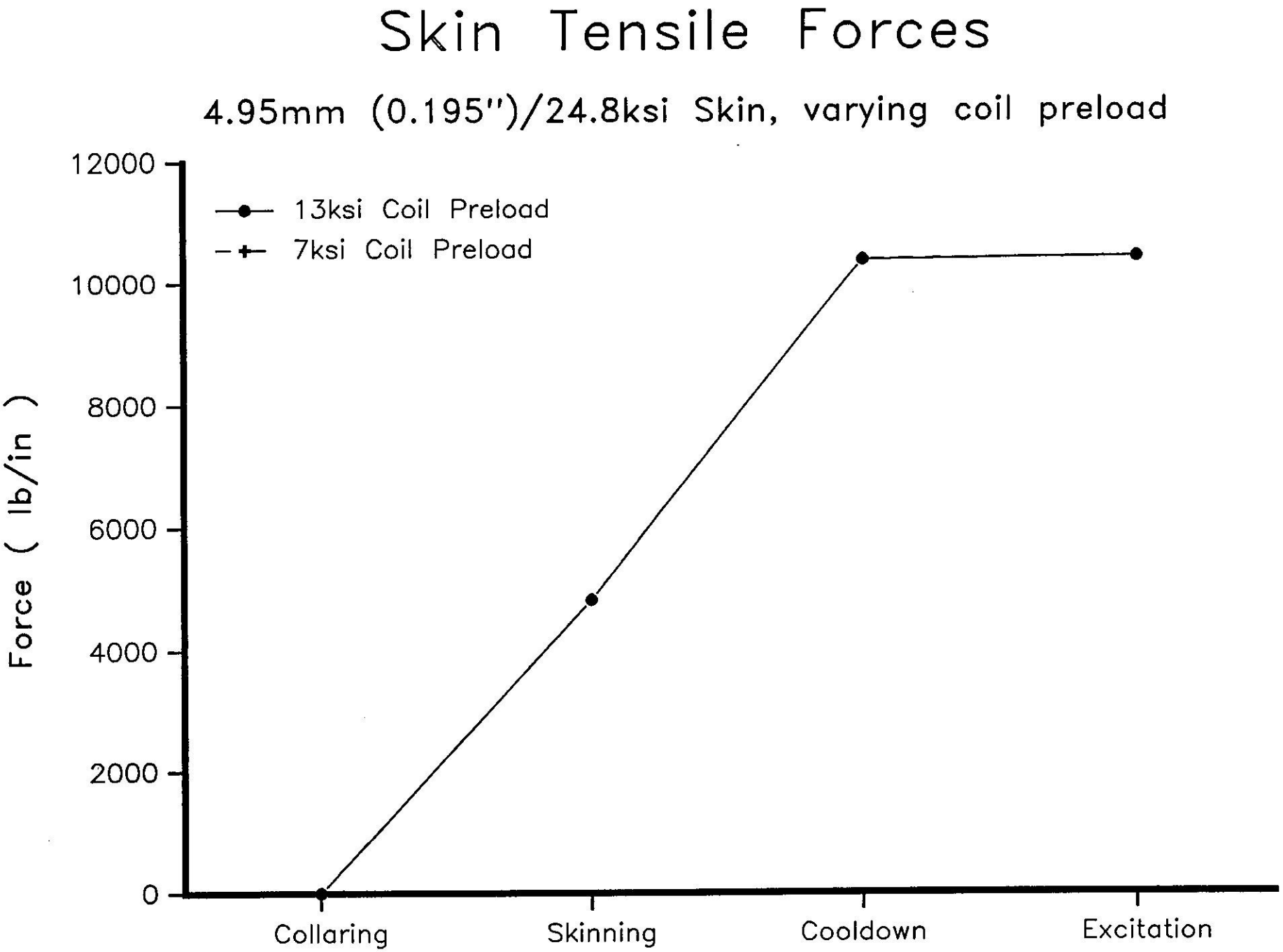
Skin Tensile Forces
4.95mm (0.195")/24.8ksi Skin, varying coil preload
13ksi Coil Preload
7ksi Coil Preload
Force (lb/in)
12000
10000
8000
6000
4000
2000
0
Collaring
Skinning
Cooldown
Excitation

Figure 10

Table 4.Collar Radial Displacements

Comparison of Collar only, complete, and SAPIV models

Preload	Horizontal	Vertical
Collar only	-0.67 (-.017)	4.59 (.117)
24.8ksi Skin	-0.68 (-.017)	4.60 (.117)

Skinning	Horizontal	Vertical	ΔH	ΔV
Collar only	-0.67 (-.017)	4.59 (.117)	0.00	0.00
24.8ksi Skin	-5.98 (-.152)	7.58 (.193)	-5.30	2.98

Cooldown	Horizontal	Vertical	ΔH	ΔV
Collar only	-8.99 (-.228)	-4.47 (-.114)	-8.32	-9.06
24.8ksi Skin	-11.91 (-.302)	-2.87 (-.073)	-5.93	-10.45
SAPIV				-5.8

Excitation	Horizontal	Vertical	ΔH	ΔV
Collar only	-4.35 (-.111)	-7.81 (-.198)	4.64	-3.34
24.8ksi Skin	-11.21 (-.285)	-4.06 (-.103)	0.70	-1.19
SAPIV			2.5	-1.7

VERTICAL SPLIT YOKE (1/4 INCH SHELL, LORENTZ FORCE EFFECT, COLD)

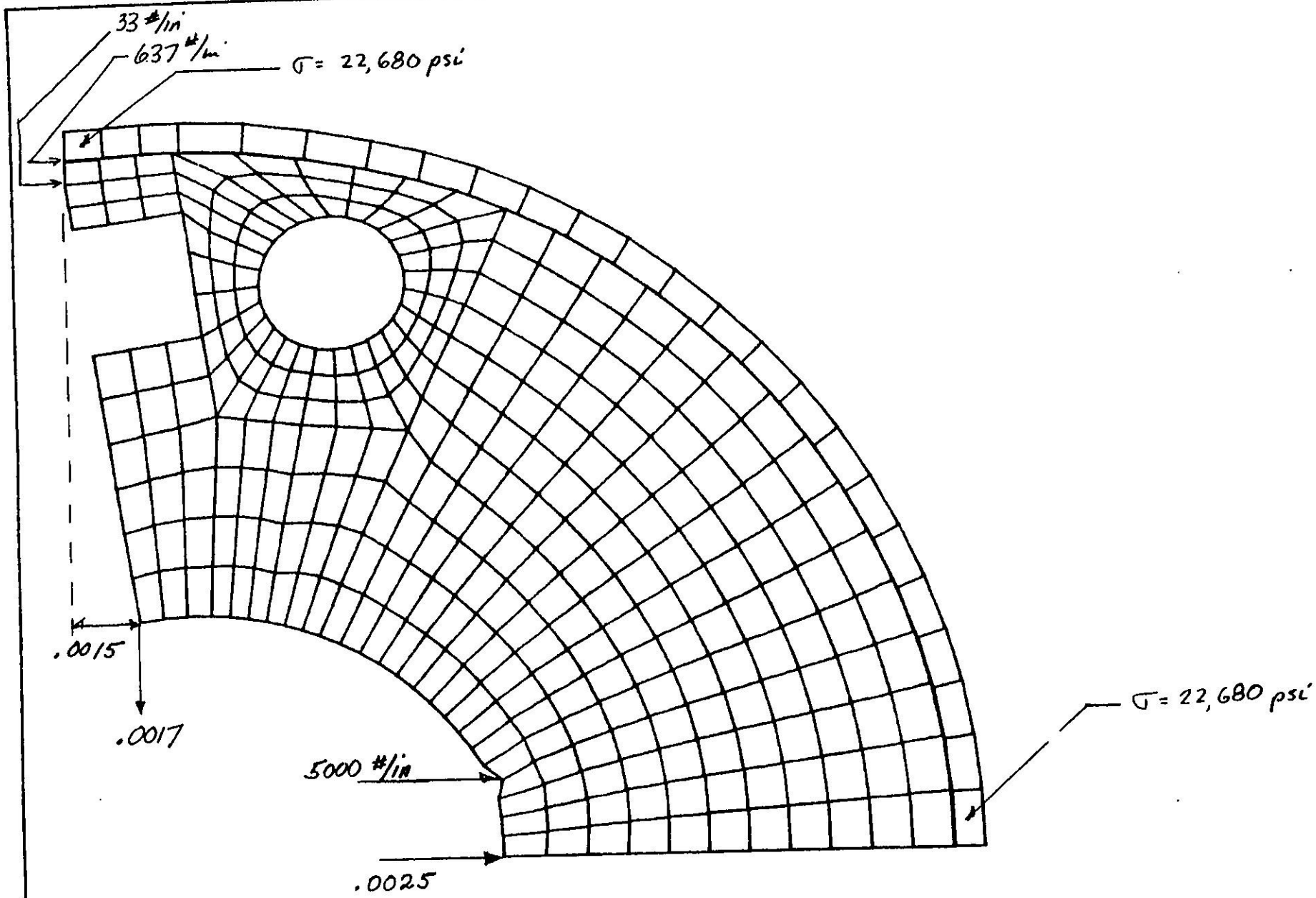

Figure 11

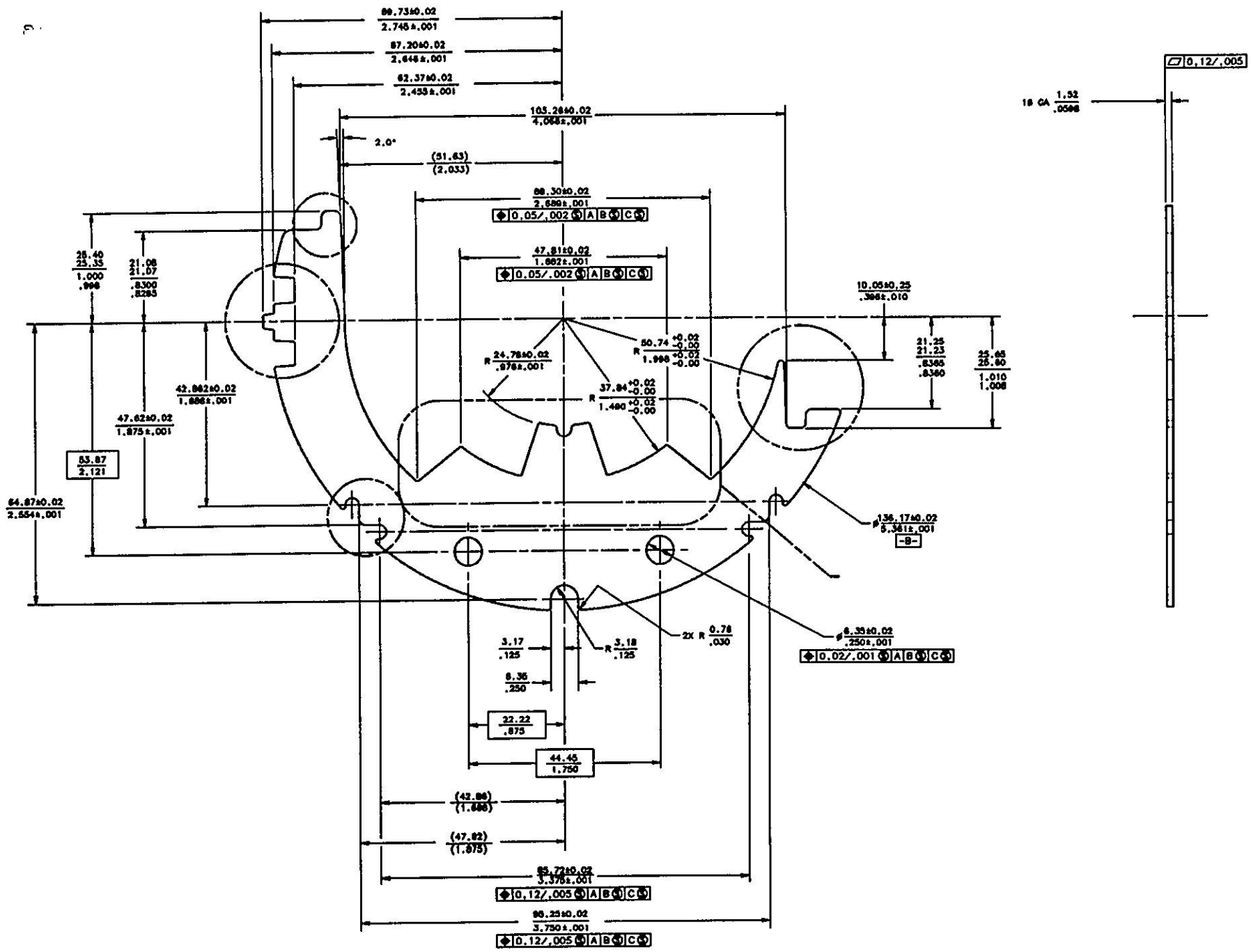
69.73±0.02
2.745±.001
67.20±0.02
2.645±.001
62.37±0.02
2.455±.001
105.26±0.02
4.068±.001
2.0°
(51.63)
(2.033)
68.30±0.02
2.689±.001
0.05/.002 A B C
47.81±0.02
1.882±.001
0.05/.002 A B C
25.40
25.35
1.000
.998
21.08
21.07
.8300
.8295
42.862±0.02
1.686±.001
47.62±0.02
1.875±.001
53.87
2.121
64.87±0.02
2.554±.001
R 24.78±0.02
.976±.001
R 50.74 +0.02 -0.00
1.998 +0.02 -0.00
R 37.84 +0.02 -0.00
1.490 +0.02 -0.00
10.05±0.25
.396±.010
21.25
21.23
.8365
.8360
25.65
25.60
1.010
1.008
ø136.17±0.02
5.361±.001
-B-
2X R 0.78
.030
ø6.35±0.02
.250±.001
0.02/.001 A B C
3.17
.125
R 3.18
.125
6.35
.250
22.22
.875
44.45
1.750
(42.86)
(1.686)
(47.62)
(1.875)
85.72±0.02
3.375±.001
0.12/.005 A B C
95.25±0.02
3.750±.001
0.12/.005 A B C
18 GA 1.52
.0598
0.12/.005

Figure 12

FERMILAB	O.G.P. OQ-20 OPTICAL CONTOUR PROJECTOR	INSPECTOR Steve Merkler	DATE 09/18/1990
SUBJECT PART# ME-292859 Rev. A 96C 58mm COLLAR LAM. W/O SHIMS VERTICALLY SPLIT YOKE		RECEIVED 09/13/90	SAMPLE 1A

NUMBERS.....=SURFACE NO.

RAD OF ARCS

SURF#	NOM	ACT	DEV
19	1.4930	1.4925	-.0005
23	2.0010	2.0008	-.0002
63	2.6700	2.6700	-0.0000
100	.1280	.1283	.0003
101	.1280	.1283	.0003

DRAWING SCALE

0.000 0.063 0.125 0.250 0.500

0.000 0.001 0.002 0.008

PLOT SCALE

ANGLES

SURF#	NOM	ACT	DEV
3	38.6618	38.6651	.0033
7	72.0730	72.0384	-.0346
17	287.9260	287.9289	.0029
21	321.3380	321.3561	.0181
25	272.0070	272.1535	.1465
69	3.0000	3.0151	.0151
73	177.0000	177.0568	.0568
77	171.4120	171.1733	-.2387
81	8.5880	8.8344	.2464
85	3.0000	3.1817	.1817
89	177.0000	177.0891	.0891
99	272.0000	271.9565	-.0435

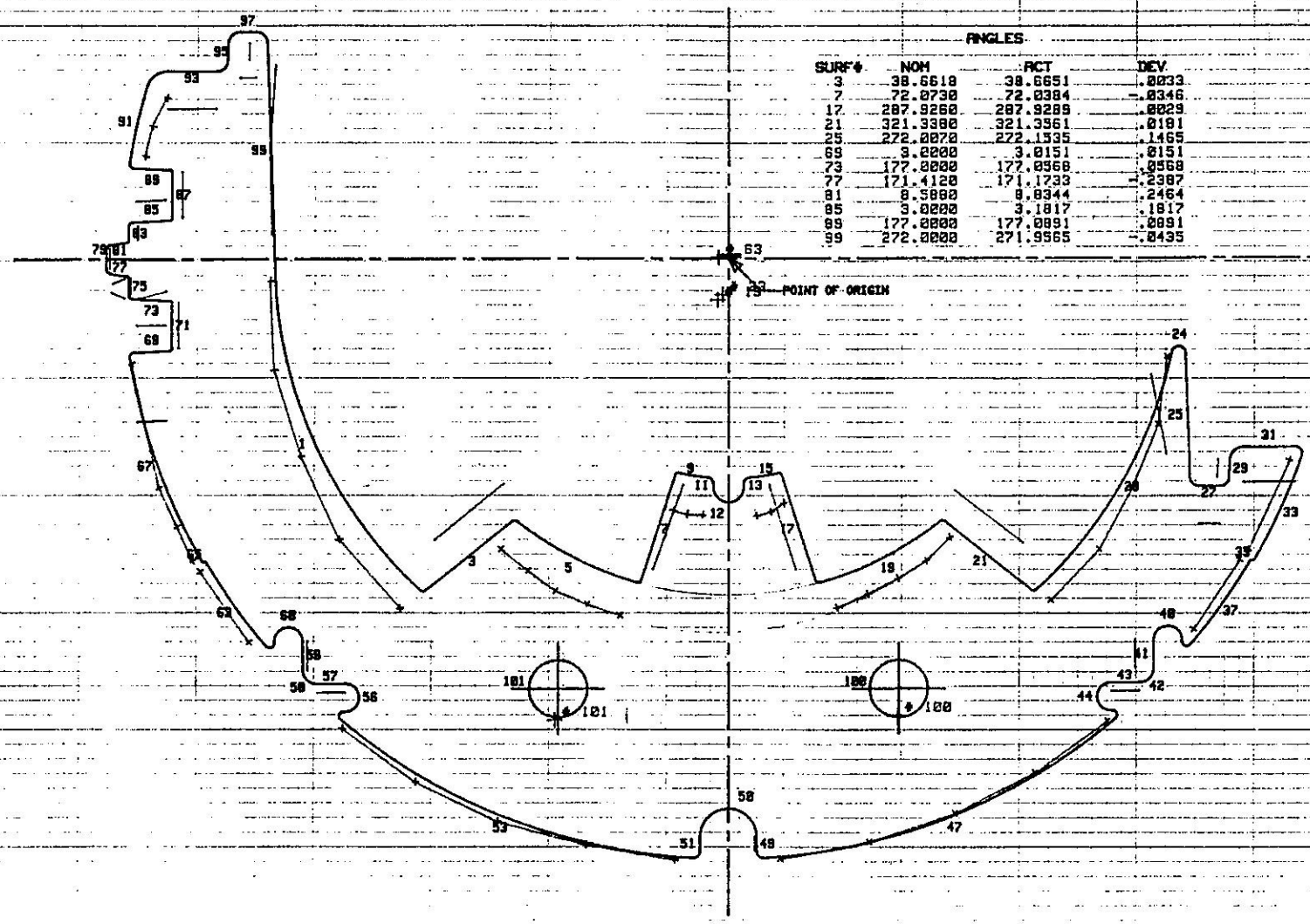

Figure 3

Distribution:

FNAL
- R. Bossert
- J. Carson
- S. Delchamps
- S. Gourlay
- W. Koska
- M. Lamm
- G. Pewitt
- M. Wake

LBL
- R. Schermer

SSCL
- C. Goodzeit
- N. Hassan
- J. Jayakumar
- R. Palmer
- G. Spigo
- J. Turner